

Research Article

Influencing Factors and Prediction Model for the Antierosion Performance of Cement-Improved Loess Compacted Using Different Compaction Methods

Kejia Yuan , Yingjun Jiang , Luyao Cai , Jiangtao Fan , Changqing Deng ,
and Jinshun Xue 

Key Laboratory for Special Area Highway Engineering of Ministry of Education, Chang'an University, South 2nd Ring Rd., Middle Section, Xi'an, Shaanxi 710064, China

Correspondence should be addressed to Yingjun Jiang; yyj@chd.edu.cn

Received 8 May 2021; Accepted 22 July 2021; Published 6 August 2021

Academic Editor: Shengwen Tang

Copyright © 2021 Kejia Yuan et al. This is an open access article distributed under the Creative Commons Attribution License, which permits unrestricted use, distribution, and reproduction in any medium, provided the original work is properly cited.

To analyze the antierosion performance of cement-improved loess (CIL), several influencing factors have been investigated based on two different compaction methods, which include the quasi-static compaction method (QSCM) and the vertical vibration compaction method (VVCVM). Then, a prediction model for the cumulative erosion mass loss (CEML) has been established. The effects of erosion on the strength deterioration of CIL were also studied. The results show that, compared with QSCM, specimens compacted using the VVCVM have better antierosion performance. As the cement content and the compaction coefficient are increased by 1%, the antierosion performance is increased by 16% and 6.2%, respectively. The eroding time has a significant effect on the antierosion performance of CIL, and the CEML increases linearly with an increase in the eroding time. The compressive strength of CIL decreases significantly due to erosion, and based on the average deterioration degree of the specimens, the design criteria for strength of CIL are proposed, which can provide reference for the design of CIL.

1. Introduction

In recent decades, loess has become an invaluable material in the construction of intercity railways. However, in its application, the unique porous structure of loess makes it vulnerable to water erosion. When the subgrade is exposed to adverse climate and hydrological conditions for a long time, a hydrodynamic load formed by the accumulated water under the traffic load is repeatedly applied to the subgrade filler. When the cohesion of the subgrade filler is less than the shear stress from the hydrodynamic load, the fine particles on the surface of the base are removed, which results in a deterioration in the performance of the subgrade in service and thus affects the safety of train operations.

To find methods of improving the erosion resistance of the subgrade, studies have researched how the strength of the subgrade filler could be improved and how eroding tests could be optimized according to the actual situation of the

subgrade and have proposed antierosion measures. In particular, extensive attention has been paid to efforts that seek to improve the strength of subgrade materials, and some chemical binders, such as cement [1–4], lime [5], nano-MgO [6], coal ash [7], fiber [8], marine-dredged soil [9], sustainable regenerated binding materials [10], and manganese slag [11], have been applied to the subgrade to investigate their effect on the water stability and the erosion resistance of the soil subgrade. Researchers at home and abroad have found that using the aforementioned materials (especially cement) not only greatly increases the strength of the subgrade, but also additionally improves the water damage resistance. Furthermore, Narloch and Woyciechowski found that specimens that have a cement content of not less than 6% show almost no symptoms of water erosion [4].

Other scholars have conducted tests using different erosion test methods [12–14]. In France, a rotary brush made of steel wire, which originated from the French roads

department, was applied to test the antierosion performance of a specimen. Specifically, the rotary wire brush was used to continuously brush the surface of the specimen, and the erosion mass of each specimen was used as the index for evaluating the antierosion performance. But the results of these studies were not in accordance with a real-life situation given that water was not involved in the test process [15]. In Australia, a vibration platform was applied to test the erosion resistance, and a specimen, which had been placed inside a steel cylinder, was vibrated using the vibration platform. The water erosion and the pumping caused by the hydrodynamic load were also considered during the test [16]. In China, an experimental method for studying the erosion resistance of semirigid base materials using the material testing system (MTS) was proposed, and this method has been compiled into the *Test Methods of Materials Stabilized with Inorganic Binders for Highway Engineering* (JTG E51-2009) [17]. Recently, some new approaches have been taken in evaluating the water damage, and the antierosion performance of inorganic-binder-stabilized soil has also been put forward [13, 14]. In addition, some scholars have also sought to establish the correlation function between the materials stabilized using an inorganic binder and the erosion parameters, and an erosion prediction model has been proposed, based on the analysis of the eroding test [18].

The aforementioned research has focused mostly on the erosion resistance of cement-stabilized materials compacted using the standardized test method: hammer quasi-static compaction method (QSCM). However, studies have indicated that the mechanical properties of the specimens compacted using QSCM are not consistent with that of field core samples, due to the renovation of compaction equipment, and their correlation is less than 70% [19–21]. Therefore, the standardized test method cannot accurately predict the mechanical properties of cement-stabilized materials. In China, vertical vibration compaction method (VVCM) is another compaction method proposed based on the principle of vibration compaction equipment and the actual compaction conditions, and the aforementioned correlation is as high as 90%, thus attracting increasing attention in recent years [22]. VVCM has been widely applied in the mechanical properties of cement improved loess (CIL), while the application of VVCM in the erosion resistance for CIL has rarely been studied.

To address this gap in the research, it is necessary to investigate the erosion resistance of CIL compacted using the VVCM and QSCM. Moreover, cement improved loess (CIL) is a complex that is composed of many materials, and its antierosion properties are closely correlated with its composition characteristics, including cement content, compaction coefficient, and eroding time. Therefore, this study, which is based on the Xi'an-Hancheng intercity railway project, has conducted a systematic and comprehensive study on the factors that influence the revealing of the erosion mechanism of CIL, and a prediction model for the cumulative erosion mass loss (CEML), based on the influencing factors, has been established. In addition, the effects of erosion on the strength deterioration of CIL have

also been studied, because they can significantly affect the design criteria for strength of CIL.

2. Materials and Test Methods

2.1. Materials. The physical properties of the site in which the loess specimens used in this study were obtained are shown in Table 1. The cement used was Portland cement P-O 42.5, produced by Shaanxi city. The specific standard is in accordance with *Common Portland Cement* (GB175-2007) [23] and the technical indicators of this cement are listed in Table 2.

2.2. Specimen Preparation Methods. In this study, the antierosion properties of CIL were investigated using specimens that had been fabricated using two compaction methods: the vertical vibration compaction method (VVCM) and the hammer quasi-static compaction method (QSCM). The cement content (mass fraction) was 2%, 3%, 4%, and 6% and the compaction coefficient was 0.92, 0.95, and 0.97, respectively.

2.2.1. VVCM. VVCM involves two procedures. First, the maximum dry density and optimum water content were determined, and then the specimen was fabricated with different compaction coefficients. In this study, the cylindrical specimens ($\Phi 100 \text{ mm} \times h 100 \text{ mm}$) were compacted using vertical vibration testing equipment (VVTE) [19, 20]. The VVTE crucial in VVCM is displayed in Figure 1, and the working parameters of VVTE based on previous research are presented in Table 3 [21, 22, 24]. The vibration compaction time of CIL specimens in the aforementioned compaction coefficients was determined by controlling the height of specimens.

2.2.2. QSCM. To determine the maximum dry density and optimum water content of CIL, specimens ($\Phi 100 \text{ mm} \times h 100 \text{ mm}$) were fabricated per the heavy compaction test (HCT-Z1) in the *Code for Soil Test of Railway Engineering* (TB10102-2010) [25]; the technical parameters of HCT-Z1 are listed in Table 4. In a similar way, QSCM was applied to prepare testing specimens ($\Phi 100 \text{ mm} \times h 100 \text{ mm}$).

2.2.3. Specimen Preparation Procedure. After having been compacted using VVCM and QSCM, the specimens were demolded and placed into a standard curing room with a temperature of $(20 \pm 2)^\circ\text{C}$ and a humidity of 95%. According to the strength-growth equation of the CIL [26], the compressive strength at 28 days is 80% of the ultimate strength, and so 28 days has been taken as the curing age of the specimen in the erosion resistance test.

2.3. Erosion Resistance Test. In the erosion resistance test (ERT), a newly developed scouring test device was used. The schematic diagram of the ERT is detailed in Figure 2, and the erosion testing equipment is illustrated in Figure 3. The erosion test comprises three parts: the system for

TABLE 1: Physical properties of loess.

Collapsibility grade of loess	Density (g/cm ³)	Liquid limit (%)	Plastic limit (%)	Plasticity index	Passing ratio (by mass) as a function of sieve size (%)				
					0.25–0.075	0.075–0.05	0.05–0.01	0.01–0.005	≤0.005
IV	2.74	26.4	15.7	10.7	2.47	7.22	53.43	13.83	23.05

TABLE 2: Technical indicators of cement.

Test index	Surface area ratio (Blaine method) (m ² /kg)	Soundness (mm)	Setting time (min)		Compressive strength (MPa)		Flexural strength (MPa)	
			Initial time	Final time	3 d	28 d	3 d	28 d
Results	329	2.05	219	426	22.3	48.2	5.8	8.06
Specific requirement	≥300	≤5.0	≥45	≤600	≥17.0	≥42.5	≥3.5	≥6.5

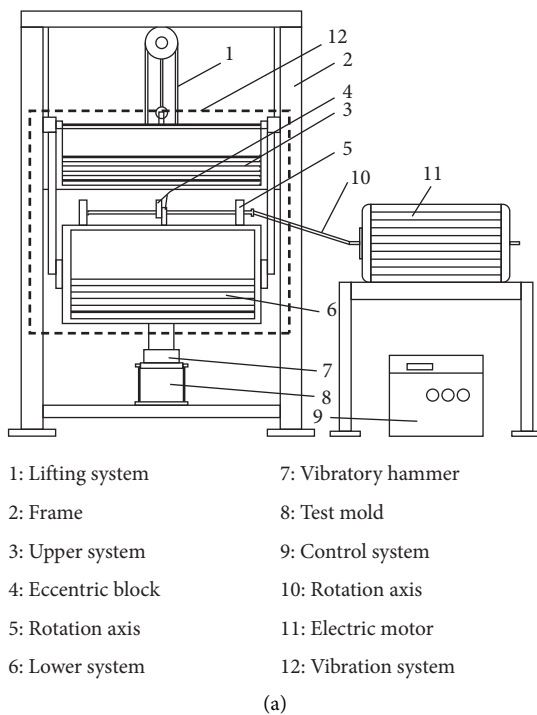


FIGURE 1: The structure of VVTE. (a) Diagram of VVTE. (b) Photograph of VVTE in laboratory.

TABLE 3: Working parameters of vertical vibration testing equipment (VVTE).

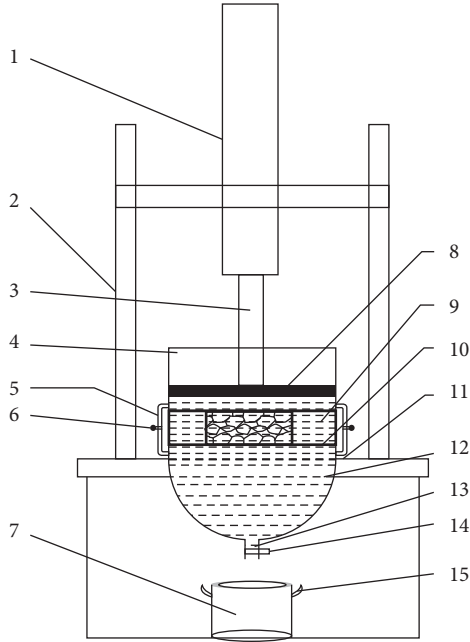
Frequency (Hz)	Nominal amplitude (mm)	Mass (kg)		
		Upper system	Lower system	Working weight
35	1.2	120	180	300

generating erosion pressure, the control system, and a container for the testing specimen. The scouring effect of the hydrodynamic load generated by pumping on the railway filler during the process of train operations can be better simulated in the scouring container by installing a telescopic rod connected with a piston under the stress loading device. The control console is equipped with a temperature control knob and a frequency control knob, which can be adjusted to simulate the antierosion

performance of the railway filler under different temperatures and working conditions. The outer wall of the scouring container is also provided with a water circulation pipeline and a water flow regulating valve. The speed of water circulation can be altered by controlling the water flow regulating valve to adjust the hydrodynamic pressure on the specimen during the scouring process and to judge the antierosion performance of railway filler under different hydrodynamic loads.

TABLE 4: The standard technical parameters of the heavy compaction test (HCT-Z1).

Mass (kg)	Compaction device specifications					Testing conditions			
	Hammer		Compaction mold			Com paction work (kJ/m ³)	Number of layers	Striking times	Maximum particle size (mm)
Bottom diameter (mm)	Drop distance (mm)	Inner diameter (mm)	Height (mm)	Volume (mm)					
4.5	51	457	102	116	947.4	2659	5	25	5



- 1: Stress loading device
- 2: Bracket
- 3: Telescopic rod
- 4: Top cover
- 5: Water circulation pipeline
- 6: Water flow regulating valve
- 7: Recyclable container
- 8: Piston
- 9: Plate for placing specimens
- 10: Base used to fix the plate
- 11: Temperature sensor
- 12: Honeycomb shaped iron mesh
- 13: Leak
- 14: Valve for water recovery
- 15: Handle of the recyclable container

FIGURE 2: Schematic diagram of the erosion test.

Given that ERT was not included in the *Code for Soil Test of Railway Engineering* (TB 10102-2010) [25], it was conducted following the method proposed in the *Test Methods of Materials Stabilized with Inorganic Binders for Highway Engineering* (JTG E51-2009) [27]. Before the test, the cured specimen was immersed in water for 24 hours before placing



FIGURE 3: Erosion testing equipment.

into the scouring container. Afterward, the scouring container was firmly placed on the testing machine, and water was injected into the container until the height of the water was 5 mm higher than the top surface of the specimen. During the test, the hydrodynamic load was 60 kPa and the scouring frequency was 100 times/min. The scoured mud was poured into the container at 5 min intervals and was allowed to precipitate for 12 hours before being dried and weighed. The test was terminated after 30 minutes of scouring. Three replicate specimens were used in the test, and the erosion resistance of CIL was evaluated using the indexes of cumulative erosion mass loss (CEML), erosion mass loss ratio (EMLR), and average erosion rate.

The EMLR was calculated according to

$$P = \frac{\sum_{i=1}^6 m_{f(i)}}{m_0}, \quad (1)$$

where P is erosion mass loss ratio of the specimen, (%), $m_{f(i)}$ is the erosion mass of the specimen at the i th time, and the CEML is the sum of $m_{f(i)}$, (g), i is the time (with each 5 min interval recorded as one time), and m_0 is the mass of the specimen.

The average erosion rate was calculated using

$$V_t = \frac{\sum_{i=1}^6 m_{f(i)}}{30}, \quad (2)$$

where V_t is the erosion rate of specimen in 30 min intervals.

2.4. Unconfined Compressive Strength. Following the *Code for Soil Test of Railway Engineering* (TB10102-2010) [25], specimens that had been cured for 27 days were immersed in

water for 24 hours, and then an unconfined compressive strength (UCS) test was conducted using a WAW-100 universal material testing machine. It should be noted that the code recommends that the loading rate should be controlled at 1 mm/min and that six replicate specimens should be tested. A photograph of the UCS test is displayed in Figure 4.

3. Results and Analysis

The results of ERT and the UCS of CIL after 28 days are detailed in Table 5, and a comparison of two specimens (with a cement content of 6% and a compaction coefficient of 0.95) before and after ERT is displayed in Figure 5. As can be seen from Figure 5, the surface of the specimen after ERT is concave, which indicates that some fine particles have eroded.

3.1. Influencing Factors on the Antierosion Performance of CIL

3.1.1. Influence of the Compaction Method. Using the results from Table 5, the EMLR and ratio of the CIL compacted using VVCM and QSCM have been calculated and are shown in Table 6, where P_v is the EMLR of the specimen compacted using VVCM for 30 minutes, and P_j is the EMLR of the specimen compacted using QSCM for 30 minutes.

As can be seen from Table 6, the EMLR of the specimen compacted using VVCM is lower than that of the specimen compacted using QSCM, which indicates that the anti-erosion performance of the CIL compacted using VVCM is appreciably better than that using QSCM. Moreover, the erosion resistance of the specimens compacted using VVCM improves more significantly as the cement content and compaction coefficient increase. Compared with QSCM, the EMLR of the CIL specimen compacted using VVCM can be reduced by at least 10%, which reveals that VVCM can significantly improve the erosion resistance of specimens.

This can be attributed to the different mechanisms involved in these two compaction methods. Compared with QSCM, VVCM has a relatively considerable effect on the structure of CIL. More specifically, the vibration load provides a more uniform distribution of the loess particles and makes the pores in the specimen smaller, the structure more compact, and the contact area between particles and the cohesion larger. However, in the process of QSCM, the compaction of the particles needs to continuously overcome the shear stress between the particles. The particles are relatively static and can rarely be filled with each other, which results in more overhead pores and a reduced cohesion between the loess particles. Therefore, it is quite difficult for the CIL specimen compacted using VVCM to be washed away under the same water erosion conditions, and hence the EMLR is reduced.

3.1.2. Influence of the Cement Content. In this test, four cement contents (2%, 3%, 4%, and 6%) were used to investigate the effect of the cement content on the antierosion performance of CIL. The test results are illustrated in



FIGURE 4: Photograph of an unconfined compressive strength test.

Figure 6. As can be seen, the cement content had a remarkable effect on the antierosion performance. Specifically, the antierosion performance of CIL increases with an increase in the cement content. When the cement content is less than 4%, the EMLR of CIL is reduced by 19% as the cement content is increased by 1%; for a cement content of more than 4%, the EMLR is reduced by 14% as the cement content increases by 1%, and the average decrease of EMLR is 16%. With an increase in the cement content, the hydration products and the strength of CIL are also increased, thereby improving the erosion resistance of CIL. Moreover, when the cement content exceeds 4%, there is only a relatively small effect of increasing the cement content on the improvement of CIL's erosion resistance, which can be attributed to the fact that as the cement content increases, excessive hydration heat is produced in the process of hydration. This increases the stiffness of CIL and leaves it prone to cracking, and such cracking would greatly weaken its erosion resistance. The findings in Figure 6 are in accordance with the results of Narloch and Guo [4, 18].

3.1.3. Influence of the Compaction Coefficient. Figure 7 shows the effects of the compaction coefficient on the erosion resistance of CIL. As can be seen, the EMLR and the average erosion rate of CIL prepared using VVCM and QSCM are remarkably linear in terms of the compaction coefficient. When the compaction coefficient is increased by 0.01, the EMLR of the specimens prepared using VVCM and QSCM decreases by an average of 6.2% and 7.2%, respectively, which indicates that the erosion resistance of the CIL can be significantly improved by increasing the compaction coefficient. These findings are generally consistent with the research that shows that the cement-treated mixture's antiscouring properties can be enhanced through an increase of the compaction coefficient (less than 98%) [18]. In addition, the average erosion rate of the vertical compacted CIL with a compaction coefficient of 0.95 and a cement content of 2% is 4.5 g/min, which is the same as the average erosion rate of 4.5 g/min for the specimen with a compaction coefficient of 0.92 and a cement content of 4%. Hence, it may

TABLE 5: Results of ERT and UCS of CIL.

Compaction method	Compaction coefficient	Cement content (%)	UCS (28 d) (MPa)	CEML of CIL (g) under the following eroding time (min)						P (%)	V _t (g/min)
				5	10	15	20	25	30		
VVCМ	0.92	2	1.13	35.5	57.7	88.6	125.9	162.8	204.3	12.6	6.8
		3	1.47	27.5	53.8	74.5	100.6	132.8	168.6	10.4	5.6
		4	1.62	24.8	44.8	62.5	88.6	111.6	134.5	8.2	4.5
		6	2.29	20.8	34.9	52.2	70.5	82.1	96.4	5.8	3.2
	0.95	2	1.53	22.7	41.1	61.6	81.5	108.4	134.3	8.3	4.5
		3	1.82	18.4	34.4	49.3	69.2	89.1	107.1	6.6	3.6
		4	2.22	14.7	28.7	39.1	54.7	67.0	77.3	4.7	2.6
		6	2.68	10.8	17.2	26.5	36.3	43.5	50.3	3.0	1.7
	0.97	2	2.00	16.7	27.4	44.0	58.7	76.9	100.2	6.1	3.3
		3	2.46	12.6	23.3	31.2	47.2	59.7	69.8	4.2	2.3
		4	2.74	8.7	16.5	22.6	31.5	38.8	45.8	2.7	1.5
		6	3.39	6.0	10.0	15.2	20.8	24.4	31.9	1.9	1.1
QSCM	0.92	2	1.03	38.3	65.2	101.9	137.2	175.8	222.7	14.0	7.4
		3	1.30	31.1	60.3	81.2	115.7	150.1	182.1	11.4	6.1
		4	1.49	27.0	51.1	71.9	99.2	122.8	148.0	9.2	4.9
		6	2.03	22.9	38.0	59.0	76.8	91.1	107.2	6.6	3.6
	0.95	2	1.34	27.9	48.1	74.5	100.2	127.9	162.5	9.9	5.4
		3	1.60	21.9	41.6	57.2	82.4	106.9	126.4	7.6	4.2
		4	1.90	17.4	33.6	46.9	63.4	79.1	94.7	5.7	3.2
		6	2.44	12.6	21.2	32.6	42.5	51.3	61.0	3.6	2.0
	0.97	2	1.65	20.9	35.6	56.3	74.6	95.3	124.3	7.4	4.1
		3	2.03	15.7	30.3	40.6	58.5	76.4	90.7	5.4	3.0
		4	2.26	11.0	20.8	28.7	39.1	48.5	57.4	3.4	1.9
		6	2.80	7.5	12.8	19.2	26.0	31.2	38.9	2.3	1.3

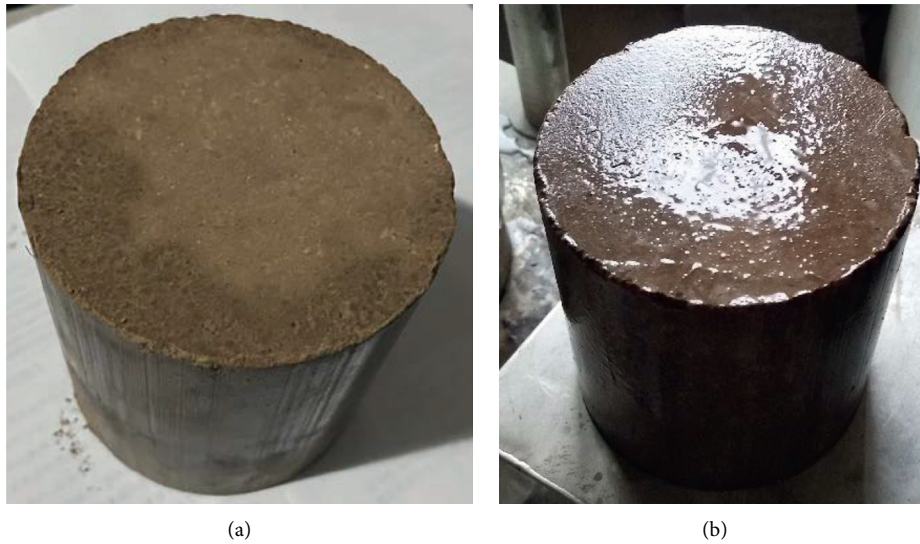


FIGURE 5: Photographs of specimens before and after the eroding test. (a) Specimen not tested in the eroding test. (b) Specimen after an eroding test for 30 min.

be appropriate to consider increasing the compaction coefficient given that it may not be economical, once the cement content reaches a certain value, to improve the antierosion performance of CIL by continuing to increase the cement content.

These results can be explained by two reasons: The first depends on the appearance of the specimen: with an increase in the compaction coefficient of the CIL, the appearance of

the specimen becomes smoother, and the resistance exerted on the surface of the specimen under the action of water erosion is reduced, so that the scouring effect on the fine particles also decreases. Second, with the increase of compaction coefficient, the soil particles in the specimen are arranged more compactly, the internal pores are decreased, and the contact area of soil particles is increased, thus showing that the internal friction angle and the cohesion of

TABLE 6: EMLR and ratio of CIL compacted using VVCM and QSCM.

Cement content (%)	EMLR and ratio of CIL with the following compaction coefficient (%)								
	0.92			0.95			0.97		
	P_v	P_j	P_v/P_j	P_v	P_j	P_v/P_j	P_v	P_j	P_v/P_j
2	12.6	14.0	0.90	8.3	9.9	0.84	6.1	7.4	0.82
3	10.4	11.4	0.91	6.6	7.6	0.87	4.2	5.4	0.78
4	8.2	9.2	0.89	4.7	5.7	0.82	2.7	3.4	0.79
6	5.8	6.6	0.88	3.0	3.6	0.83	1.9	2.3	0.83

CIL are increased, which makes it difficult for the soil particles to be washed away; therefore, the antierosion properties are improved.

3.1.4. Influence of the Eroding Time. The effects of the eroding time on the CEML of CIL are displayed in Figure 8. It can be seen that the effects of the eroding time on the CEML of CIL with different cement contents (2%, 3%, 4%, and 6%) are consistent, which indicates that there is a good linear correlation between the eroding time and the CEML of CIL. Moreover, these findings are in agreement with research that showed that there is an overall increase in the erosion of cement-bentonite when there is an increase in the erosion time [2].

3.2. Prediction Model. Based on the results that show a linear relationship between the eroding time and the antierosion performance of CIL (when the cement content is within the range of 2%~6%, the compaction coefficient is within the range of 0.92~0.97, and the eroding time is within the range of 0~30 min), the linear prediction model shown in equation (3) has been established to collate and predict the experimental data; the predicted results are shown in Table 7:

$$m_f = S \times T, \quad (3)$$

where m_f is the CEML of specimen (g), S is the scouring coefficient of the specimen, and T is the eroding time of specimen (min).

As shown in Table 7, the correlation coefficient R^2 of $P \sim T$ was 0.99, which indicates the feasibility of the linear function. The scouring coefficient decreases accordingly as the cement content and compaction coefficient increase. In addition, based on the previous analysis, the CEML of specimen increases linearly with an increase in the cement content and compaction coefficient. Therefore, the erosion resistance of the specimen can be predicted and calculated according to equation (4); the predicted results are given in Table 8.

$$S = a \times P_s + b \times K + c \times P_s \times K + d, \quad (4)$$

where P_s is the cement content of the specimen (%); K is the compaction coefficient of the specimen; a is the predicted parameter representing the effects of the cement content on erosion resistance of CIL; b is the predicted parameter representing the effects of the compaction coefficient on the

erosion resistance of CIL; c is the predicted parameter representing the interaction of the cement content and the compaction coefficient on the erosion resistance of CIL; and d is the intercept.

To verify the accuracy of the prediction model, some experimental data of the ERT (30 min) of specimens with three different kinds of cement content (3%, 4%, and 6%) and three compaction coefficients (0.92, 0.95, and 0.97) of specimen were selected to test the prediction model and calculate the relative errors. The comparison between the predicted data and the measured data is shown in Figure 9.

As can be seen from Figure 9, the relative errors between the predicted data and the measured data are between 0 and 15%, with an average value of 1.34%. This meets the requirements of codes ($\leq 20\%$) [25], thereby indicating that the predicted results of the prediction model are in good agreement with the measured results. Therefore, this model can be applied to the prediction of the CEML of CIL.

3.3. Relationship between the Antierosion Performance and UCS of CIL. The correlation between the CEML of a specimen with an eroding time of 30 min and the UCS of a specimen at a curing age of 28 days is plotted in Figure 10. As can be seen, there is a strong negative correlation between CEML and UCS, and the correlation between the CEML and the UCS conforms to the following boundary conditions: when the m_f is 0, the UCS of a specimen at curing age of 28 days is q_{uz} ; and when the m_f is approaching infinity, the compressive strength of the specimen is almost 0.

These findings can be ascribed to the strength formation mechanism of CIL. The strength of CIL is mainly a result of the cohesion between cement and soil particles and the friction between soil particles. The cohesion of loess is closely related to various physical and chemical forces between particles, including Coulomb force (electrostatic force), van der Waals force, and cementation. The internal friction angle of loess is attributed to the interlocking force produced by the contact area and the intercalation between particles. Given that the loess used was the same throughout this study, the strength is mainly correlated with the cemented materials. When the cement content is relatively high, the cement can be evenly distributed and well wrapped around the soil particles. This will enhance the bonding force and produce a more compact structure with a higher strength within the specimen, and thus, it would be difficult for the soil particles to be washed away by the water flow. Accordingly, the CEML is reduced, and the antierosion property is improved. However, when the cement content is low, it is often difficult to evenly combine the cement slurry with soil particles, and as a result, the bonding force between the soil particles is poor and the compressive strength is reduced; thus, the soil particles are easily washed away under the hydrodynamic load, and the antierosion properties are relatively weak.

The erosion deterioration factor proposed to investigate the effects of erosion on the compressive strength was calculated using equation (5), and the results are listed in Table 9. Moreover, a comparison of the compressive strength

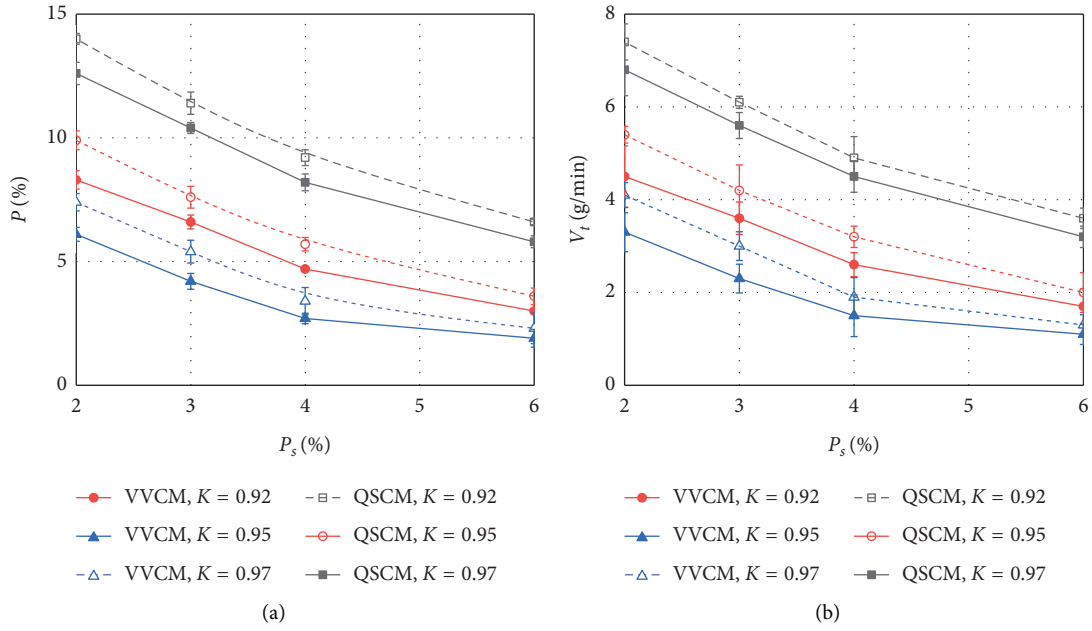


FIGURE 6: Effect of cement content on erosion resistance of CIL. (a) $P_S \sim P$. (b) $P_S \sim V_t$.

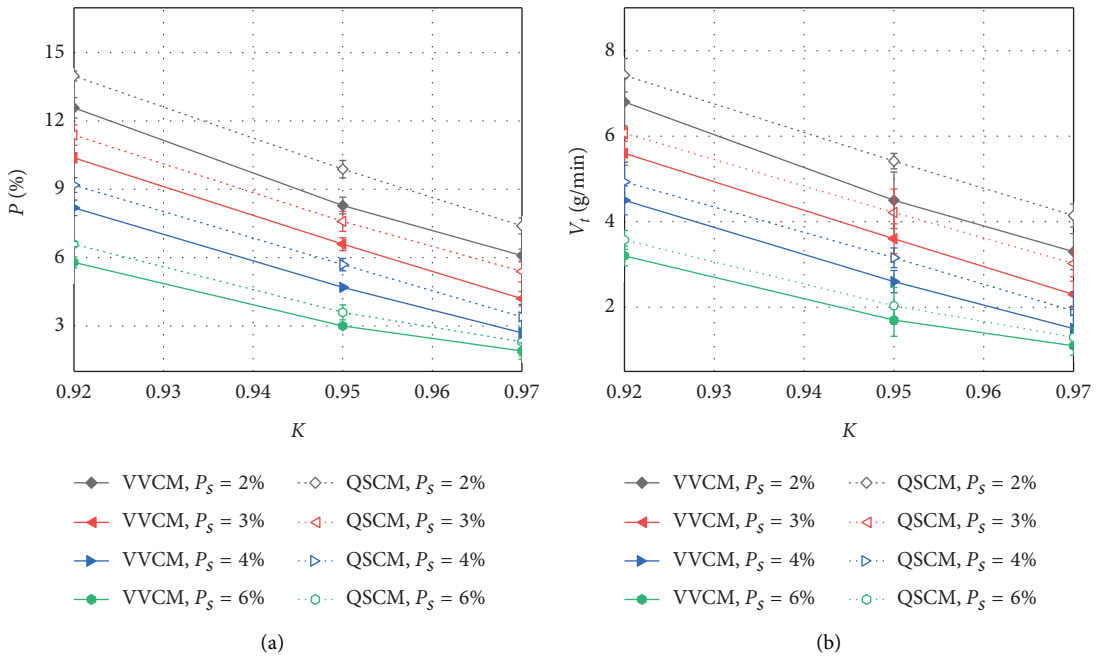


FIGURE 7: Effect of compaction coefficient on erosion resistance of CIL. (a) $K \sim P$. (b) $K \sim V_t$.

of the specimen before and after ERT is illustrated in Figure 11:

$$DR = \frac{q_E}{q_u} \times 100\%, \quad (5)$$

where DR is the erosion deterioration factor of specimen (%), q_E is the compressive strength of the specimen after ERT (MPa), and q_u is the compressive strength of the specimen (MPa).

As is evident from Figure 11, the compressive strength of CIL is significantly decreased after ERT, in which the erosion deterioration factors for specimens compacted using VVC and QSCM are 79.5% and 73.7%, respectively. This indicates that the hydrodynamic load not only has an effect on the specimen but also causes damage, to a certain extent, to the internal structure of the specimen. This produces micro-damage and microcracks inside the specimen, which causes a reduction in the compressive strength. This can be ascribed

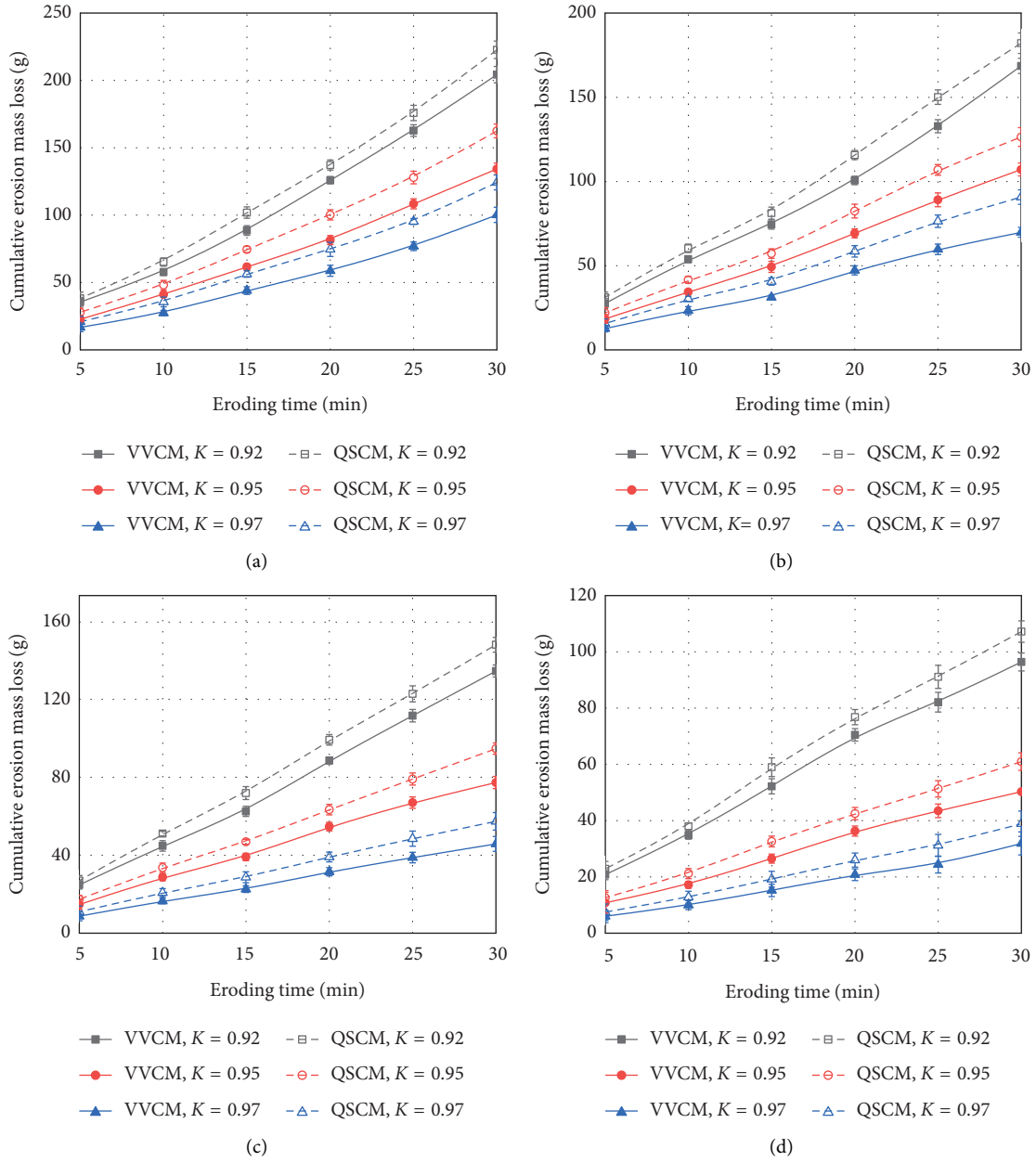


FIGURE 8: Effect of the eroding time on CEML of CIL. (a) Cement content = 2%. (b) Cement content = 3%. (c) Cement content = 4%. (d) Cement content = 6%.

TABLE 7: Predicted parameters of erosion resistance of CIL.

Compaction method	Compaction coefficient	Cement content (%)	Scouring coefficient	R^2	
VVCM	0.92	2	6.51	0.99	
		3	5.36	0.99	
		4	4.44	0.99	
		6	3.34	0.99	
		2	4.32	0.99	
		3	3.52	0.99	
	0.95	4	2.65	0.99	
		6	1.73	0.99	
		0.97	2	3.13	0.99
			3	2.33	0.99
			4	1.55	0.99
			6	1.03	0.99

TABLE 7: Continued.

Compaction method	Compaction coefficient	Cement content (%)	Scouring coefficient	R^2
QSCM	0.92	2	7.12	0.99
		3	5.94	0.99
		4	4.93	0.99
		6	3.70	0.99
	0.95	2	5.19	0.99
		3	4.17	0.99
		4	3.17	0.99
		6	2.08	0.99
	0.97	2	3.92	0.99
		3	2.99	0.99
		4	1.94	0.99
		6	1.28	0.99

TABLE 8: The predicted parameters of the scouring coefficient.

Compaction method	a	b	c	d	R^2
VVCM	-548.61	-77.51	511.40	79.12	0.98
QSCM	-416.07	-71.38	359.70	74.28	0.98

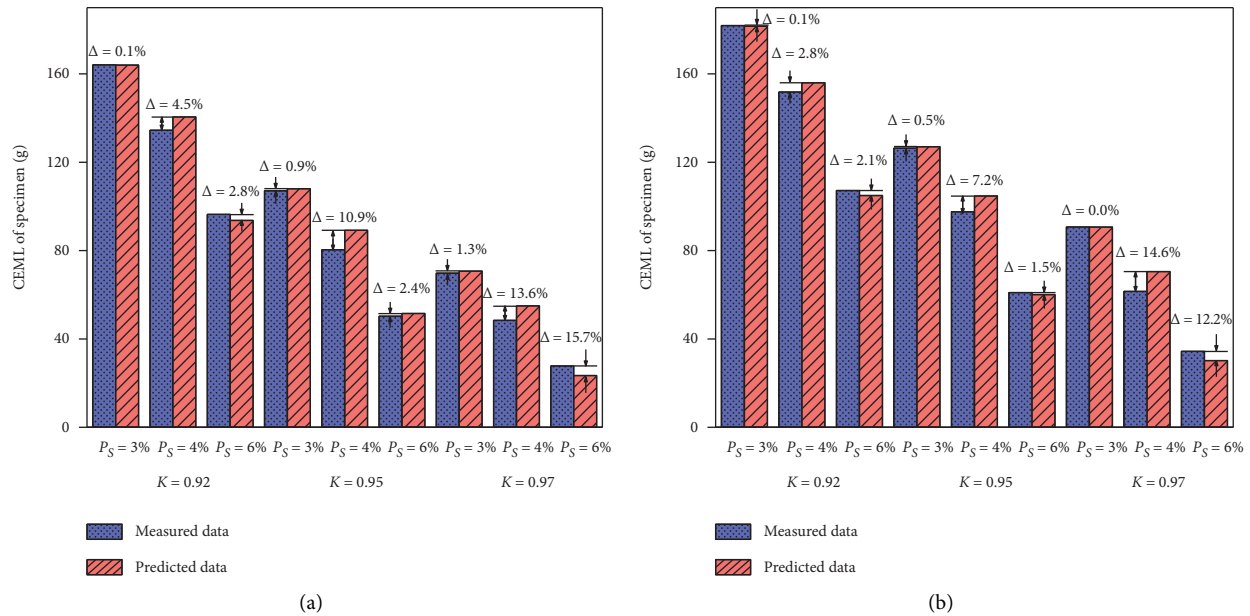


FIGURE 9: Relative errors between the predicted data and the measured data. (a) Specimen compacted using VVCM. (b) Specimen compacted using QSCM.

to the fact that the damage of CIL is caused by the process of microstructural damage. Under cyclic dynamic loading, fine particles with low cohesion are eroded first, which results in defects on the surface of the specimen. With an increase in the eroding time, the defects on the surface of the specimen deepen further, and the water content in the specimen also increases sharply. Due to the collapsibility of loess, the deterioration of the compressive strength is aggravated by the invasion and erosion of water loading. These findings are consistent with research that shows that the damage of the materials under cyclic erosion of hydrodynamic pressure is a

cumulative process that can result in the strength degradation of the material properties [13, 28–31].

3.4. Design Criteria for Strength of CIL Based on the Anti-erosion Performance. According to the Code for Design of Railway Earth Structure (TB10001-2016) [32], the UCS of CIL is used as the technical indicator in the design of subgrade materials. However, studies have indicated that the design value of UCS is calculated based on the train load, while the long-term stability under the influence of erosion

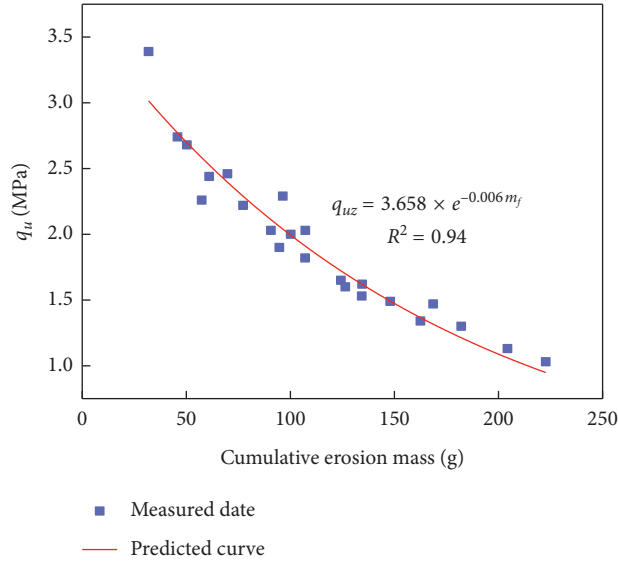


FIGURE 10: The correlation between the CEML and the UCS of CIL.

TABLE 9: The results of the compressive strength of the specimen before and after ERT.

Compaction method	Compaction coefficient	Cement content (%)	q_u (MPa)	q_E (MPa)	DR (%)
VVCМ	0.92	2	1.13	0.77	68.1
		3	1.47	1.11	75.5
		4	1.62	1.27	78.4
		6	2.29	1.79	78.2
	0.95	2	1.53	1.16	75.8
		3	1.82	1.41	77.5
		4	2.22	1.82	82.0
		6	2.68	2.26	89.2
	0.97	2	2.00	1.56	78.0
		3	2.46	1.98	80.5
		4	2.74	2.38	86.9
		6	3.39	2.96	84.4
QSCM	0.92	2	1.03	0.68	66.0
		3	1.30	0.88	67.7
		4	1.49	1.06	71.1
		6	2.03	1.49	73.4
	0.95	2	1.34	0.91	67.9
		3	1.60	1.11	69.4
		4	1.90	1.50	78.9
		6	2.44	1.94	79.5
	0.97	2	1.65	1.12	67.9
		3	2.03	1.62	79.8
		4	2.26	1.83	81.0
		6	2.80	2.30	82.1

is not considered [33]. As is detailed from Table 9 and Figure 11, the compressive strength of CIL is significantly affected by the erosion test. Therefore, the erosion deterioration characteristics should be considered. Based on the design theory of strength control, the design criteria of CIL are calculated according to equations (6) and (7):

$$[q_u] \geq \sigma_{\max}, \tag{6}$$

$$[q_u] = \eta_e \cdot q_u, \tag{7}$$

where $[q_u]$ is the strength considering the influence of erosion on CIL (MPa); q_u is the strength of CIL before erosion deterioration (MPa); η_e is the erosion deterioration factor of CIL; σ_{\max} is the maximum stress of subgrade (MPa).

The design criteria for UCS of CIL considering the antierosion performance is obtained by substituting equation (7) into equation (6):

$$q_u \geq \frac{\sigma_{\max}}{\eta_e}. \tag{8}$$

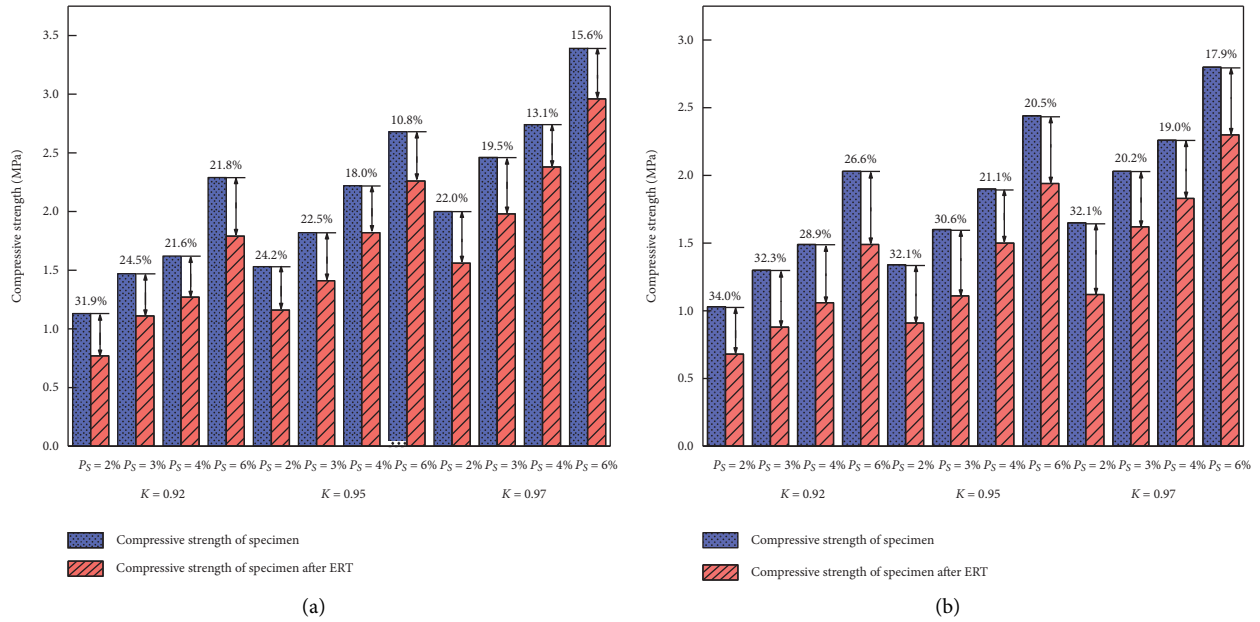


FIGURE 11: Comparison of the compressive strength of the specimen before and after ERT. (a) Specimen compacted using VVCM. (b) Specimen compacted using QSCM.

TABLE 10: The design criteria for UCS of CIL based on the antierosion performance.

Railway classification	Design speed (km/h)	Unconfined compressive strength (MPa)			
		The bottom layer of the subgrade bed Specification value	Revised value	The embankment below subgrade bed Specification value	Revised value
Ballast track	120, 160	≥0.35	≥0.48	≥0.20	≥0.28
	200			≥0.25	≥0.34
Ballastless track	250, 300	≥0.35	≥0.48	≥0.25	≥0.34
	350				

In this study, the erosion deterioration factors for specimens compacted using VVCM and QSCM are 79.5% and 73.7%, respectively. According to the *Code for Design of Railway Earth Structure* (TB10001-2016) [31], the UCS of CIL is listed in Table 10. By substituting the aforementioned stress and erosion deterioration factor into equation (8), the revised design standard for UCS of CIL can be calculated, and the results are listed in Table 10.

4. Conclusions

The influencing factors on the antierosion performance of CIL, which include the compaction method, the cement content, the compaction coefficient, and the eroding time, have been investigated systematically and prediction models of CEML have been established based on a newly developed scouring test device. The following conclusions can be drawn from this research:

- (1) Compared with QSCM, the antierosion performance of CIL compacted using VVCM can be significantly improved, and the erosion mass loss ratio can be reduced by at least 10%.
- (2) There was found to be a strong correlation between the antierosion performance of CIL and influencing

factors such as the cement content and the compaction coefficient. As the cement content and compaction coefficient were increased by 1%, the erosion resistance increased by 16% and 6.2%, respectively.

- (3) The eroding time has a significant effect on the CEML of CIL, with the CEML increasing linearly with an increase in the eroding time.
- (4) The prediction model of CEML based on the influencing factors has been established, and the correlation coefficient is higher than 90%.
- (5) The compressive strength of CIL decreases significantly due to the dynamic erosion loading. The average deterioration factor of CIL compacted by VVCM is 79.5%, and that of the specimen compacted using QSCM is 73.7%. Based on the erosion deterioration factor, the revised design criteria for strength of CIL is proposed.

The results of this investigation are of great significance in the application of loess and the improvement of subgrade durability in the construction of intercity railways. Further field erosion tests and an investigation into the micro-mechanisms of cement improved loess after ERT will be conducted.

Data Availability

The data used to support the findings of this study are included within the article.

Conflicts of Interest

The authors declare that there are no conflicts of interest regarding the publication of this paper.

Acknowledgments

This work was supported by the Science and Technology Project from Shaanxi Provincial Department of Transportation (Grant nos. 18-02K and 19-27K) and the Scientific Research of Central Colleges of China for Chang'an University (Grant no. 300102218212).

References

- [1] Y. H. Miao, W. X. Yu, Y. Hou et al., "Influences of clay brick particles on the performance of cement stabilized recycled aggregate as pavement base," *Sustainability*, vol. 10, no. 10, p. 3505, 2018.
- [2] Z. J. Wang, B. M. Zhao, and A. C. D. Royal, "Investigation of erosion of cement-bentonite via piping," *Advances in Materials Science and Engineering*, vol. 2017, Article ID 1762042, 2017.
- [3] B. Medvey and G. Dobszay, "Durability of stabilized earthen constructions: a review," *Geotechnical & Geological Engineering*, vol. 38, no. 3, pp. 2403–2425, 2020.
- [4] P. Narloch and P. Woyciechowski, "Assessing cement stabilized rammed earth durability in a humid continental climate," *Buildings*, vol. 10, no. 2, p. 26, 2020.
- [5] A. Mehenni, O. Cuisinier, and F. Masrouri, "Impact of lime, cement, and clay treatments on the internal erosion of compacted soils," *Journal of Materials in Civil Engineering*, vol. 28, no. 9, Article ID 04016071, 2016.
- [6] K. Yao, W. Wang, N. Li, C. Zhang, and L. Wang, "Investigation on strength and microstructure characteristics of Nano-MgO admixed with cemented soft soil," *Construction and Building Materials*, vol. 206, pp. 160–168, 2019.
- [7] S. Raj S, A. K. Sharma, and K. B. Anand, "Performance appraisal of coal ash stabilized rammed earth," *Journal of Building Engineering*, vol. 18, pp. 51–57, 2018.
- [8] J. Zhang, X. Z. Weng, and J. Z. Liu, "Strength and water stability of a fiber-reinforced cemented loess," *Journal of Engineered Fibers and Fabrics*, vol. 13, no. 1, pp. 72–83, 2018.
- [9] T. M. Do, G. Kang, N. Vu, and Y.-S. Kim, "Development of a new cementless binder for marine dredged soil stabilization: strength behavior, hydraulic resistance capacity, microstructural analysis, and environmental impact," *Construction and Building Materials*, vol. 186, pp. 263–275, 2018.
- [10] X. R. Zhang, W. G. Li, Z. Tang et al., "Sustainable regenerated binding materials (RBM) utilizing industrial solid wastes for soil and aggregate stabilization," *Journal of Cleaner Production*, vol. 275, Article ID 122991, 2020.
- [11] F. Qin, Z. B. He, and Q. N. Huang, "Research on the corrosion resistance of manganese slag cement stabilized macadam base," *Advanced Materials Research*, vol. 280, pp. 13–18, 2011.
- [12] A. M. Sha and L. Q. Hu, "Experimental study on the anti-erosion properties of pavement base materials," *Chinese Journal of Geotechnical Engineering*, vol. 24, no. 3, pp. 276–280, 2002.
- [13] D. Sha, B. F. Pan, Y. R. Sun et al., "A new approach to evaluating the moisture damage of semi-rigid base materials based on the eroding test by the hydrodynamic pressure generator," *Construction and Building Materials*, vol. 227, Article ID 116613, 2019.
- [14] G. M. Mutter, "Utilization of water turbidity meter devices in estimating the aggregate stability of many artificially stabilized soils," *International Journal of Integrated Engineering*, vol. 10, no. 1, pp. 9–16, 2018.
- [15] C. W. Lovel and R. A. Mutti, *Design to Prevent Pumping in concrete Pavement*, Federal Highway Administration, Washington, DC, USA, 1987.
- [16] Y. s. Jung, D. G. Zollinger, and A. J. Wimsatt, "Test method and model development of subbase erosion for concrete pavement design," *Transportation Research Record: Journal of the Transportation Research Board*, vol. 2154, no. 1, pp. 22–31, 2010.
- [17] A. M. Sha and L. Q. Hu, "Study of the testing method for anti-erosion properties of semi-rigid base materials," *China Journal of Highway and Transport*, vol. 15, no. 2, pp. 7–10, 2002.
- [18] R. Guo, T. Nian, P. Li, J. Fu, and H. Guo, "Anti-erosion performance of asphalt pavement with a sub-base of cement-treated mixtures," *Construction and Building Materials*, vol. 223, pp. 278–287, 2019.
- [19] Y. J. Jiang, K. J. Yuan, C. Q. Deng et al., "Fatigue performance of cement-stabilized crushed gravel produced using vertical vibration compaction method," *Journal of Materials in Civil Engineering*, vol. 32, no. 11, Article ID 04020318, 2020.
- [20] C. Q. Deng, Y. J. Jiang, K. J. Yuan et al., "Mechanical properties of vertical vibration compacted lime-fly ash-stabilized macadam material," *Construction and Building Materials*, vol. 251, Article ID 119089, 2020.
- [21] Y. J. Jiang, K. J. Yuan, Q. L. Li et al., "Comparison of mechanical properties of cement-stabilized loess produced using different compaction methods," *Advances in Materials Science and Engineering*, vol. 2020, Article ID 4835704, 2020.
- [22] X. Ji, Y. Hou, X. Li, and T. Wang, "Comparison on properties of cement-stabilised gravel prepared by different laboratory compaction methods," *Road Materials and Pavement Design*, vol. 20, no. 4, pp. 991–1003, 2019.
- [23] MOT (ministry of transport of the people's Republic of China), "Common Portland Cement." (GB175-2007), China Communications Press, Beijing, China, 2007.
- [24] J. L. Ren and C. Yin, "Investigating mechanical characteristics of aggregate structure for road materials," *International Journal of Pavement Engineering*, pp. 1–15, 2020.
- [25] MOT (Ministry of Transport of the People's Republic of China), "Code for Soil Test of Railway Engineering" (TB10102-2010), China Communications Press, Beijing, China, 2010.
- [26] Y. J. Jiang, Q. L. Li, Y. Yi et al., "Cement-modified loess base for intercity railways: mechanical strength and influencing factors based on the vertical vibration compaction method," *Materials*, vol. 13, no. 16, p. 3643, 2020.
- [27] MOT (Ministry of Transport of the People's Republic of China), "Test Methods of Materials Stabilized with Inorganic Binders for Highway engineering." (JTG E51-2009), China Communications Press, Beijing, China.
- [28] L. Fang, Z. P. You, A. Diab et al., "External sulfate attack on concrete under combined effects of flexural fatigue loading and drying-wetting cycles," *Construction and Building Materials*, vol. 249, Article ID 118224, 2020.

- [29] S. W. Tang, Y. Wang, Z. C. Geng, X. F. Xu, and J. T. Chen, "Structure, fractality, mechanics and durability of calcium silicate hydrates," *Fractal and Fractional*, vol. 5, no. 2, p. 47, Article ID 5020047, 2021.
- [30] L. Wang, F. X. Guo, Y. Q. Lin et al., "Comparison between the effects of phosphorous slag and fly ash on the C-S-H structure, long-term hydration heat and volume deformation of cement-based materials," *Construction and Building Materials*, vol. 250, Article ID 118807, 2020.
- [31] L. Wang, M. M. Jin, S. H. Zhou et al., "Investigation of Microstructure of C-S-H and Micro-mechanics of Cement Pastes under NH_4NO_3 Dissolution by ^{29}Si MAS NMR and Microhardness," *Measurement*, 2021.
- [32] MOT (Ministry of Transport of the People's Republic of China), "Code for Design of Railway Earth Structure" (TB10001-2016), China Communications Press, Beijing, China, [in Chinese], 2016.
- [33] Y. S. Ye, A. J. Cheng, and Q. L. Zhang, "Study on the design and compaction standard of improved soil subgrade," *China Railway Science*, vol. 29, no. 2, pp. 1-5, 2008.